Terahertz Dielectric Properties and Low-Frequency Phonon Resonances of ZnO Nanostructures

Jiaguang Han,[†] **Weili Zhang,*,**[†] **Wei Chen,**[‡] **Sanith Ray,**[†] **Jun Zhang,**[§] **Mingxia He,**[†,‖] **Abul K. Azad,**[†] **and Zhiyuan Zhu**[⊥]

School of Electrical and Computer Engineering, Oklahoma State University, Stillwater, Oklahoma 74078, Department of Physics, University of Texas at Arlington, Arlington, Texas 76019, College of Chemistry and Chemical Engineering, Inner Mongolia University, Hohhot, Inner Mongolia 010021, People's Republic of China, Center for Terahertz Waves and College of Precision Instrument and Optoelectronics Engineering, Tianjin University, Tianjin 300072, People's Republic of China, and Shanghai Institute of Applied Physics, Shanghai 201800, People's Republic of China

Far-infrared optical and dielectric properties of nanostructured ZnO of different morphologies are characterized by terahertz time-domain spectroscopy. Frequency-dependent complex dielectric function, power absorption, and refractive index are experimentally measured in the terahertz regime. The results are analyzed and well fit with dielectric theories combined with effective medium models. Different ZnO nanostructure morphologies exhibit different characteristics due to diverse resonance mechanisms dominated by either free electrons or phonons. The dielectric function of tubular and prismlike ZnO structures exhibits the Drude-like behavior, while it is dominated by the low-frequency phonon resonances for nanowires. Additionally, the overall low-frequency phonon resonances of these nanostructures are measured by Raman scattering spectroscopy, showing good consistency with those of bulk wurtzite single-crystal ZnO.

I. Introduction

There has been enormous interest in crystalline and nanostructured ZnO due to their unique properties and large span of promising applications ranging from electro-optic, acousto-optic, optoelectronic devices, ultraviolet (UV)-light emitters, chemical sensors, and piezoelectric materials.[1−4] With a direct band gap of 3.37 eV at room temperature (RT), ZnO is one of the most promising semiconductors suitable for short-wavelength optoelectronic applications.[6−9] The properly doped ZnO can be made electrically conductive and transparent in the visible spectral region, and therefore it can be used as the transparent conductive electrodes in solar cells and flat panel displays.[10] Additionally, surface acoustic wave filters made from ZnO films have been used for video and radio-frequency circuits.[11]

In the terahertz regime, ZnO possesses a number of advantages in terms of device applications, such as ease in fabrication, wide band gap, rather high mobility and resistivity, and transparency in a broad terahertz frequency range.[12−14] Pulsed terahertz radiation has been demonstrated from a photoconductive switch fabricated on high-resistivity, single-crystal ZnO.[12] The experimental result showed that its high breakdown electric field enables ZnO to be an intriguing semiconductor in high-power terahertz generation. Recently, particular attention has been paid to ZnO nanostructures not only for fundamental research on material properties in the terahertz regime but also for promising device applications.[13,15] In this article, we present experimental studies of far-infrared dielectric properties and low-frequency phonon resonances of various chemically synthesized ZnO nanostructures by terahertz time-domain spectroscopy (THz-TDS)[16] combined with high-resolution Raman spectroscopy. The measured results are analyzed on the basis of dielectric and phonon dispersion theories and effective medium models, and they are compared with those of ZnO tetrapods and wurtzite single crystals.

II. Theoretical Models

Effective Medium Theory. Since each ZnO nanostructure studied here is a composite of pure ZnO particles and air, the measured frequency-dependent complex dielectric function of such two-phase mixture composite materials are often characterized well by the effective medium theories (EMTs), in which electromagnetic interactions between pure materials and host matrixes are approximately taken into account.[15] The commonly used EMTs including the Maxwell-Garnett (MG) model, the Bruggeman (BR) model, and the simple effective medium model are briefly sketched below.

The MG effective dielectric function can be obtained through the relation

$$\frac{\epsilon_{\text{eff}} - \epsilon_{\text{h}}}{\epsilon_{\text{eff}} + 2\epsilon_{\text{h}}} = f \frac{\epsilon_{\text{m}} - \epsilon_{\text{h}}}{\epsilon_{\text{m}} + 2\epsilon_{\text{h}}} \qquad (1)$$

where ϵ_{eff}, ϵ_{h}, and ϵ_{m} are the dielectric constants of the effective medium, the host medium, and the pure inclusion studied, f is the filling factor defined by the volume ratio of pure structures and over the composites. The MG model includes interactions between the particles only through the Lorentz field, which limits its use to only small filling factors.[17] It usually describes an isotropic matrix containing spherical inclusions that are

　* Corresponding author. Phone: (405) 744-7297. Fax: (405) 744-9198. E-mail: wwzhang@okstate.edu.
　† Oklahoma State University.
　‡ University of Texas at Arlington.
　§ Inner Mongolia University.
　‖ Tianjin University.
　⊥ Shanghai Institute of Applied Physics.

Dielectric and Optical Properties of ZnO Nanoforms

J. Phys. Chem. C, Vol. 111, No. 35, 2007 **13001**

isolated from each other, such as the metal particles dispersed in a surrounding host matrix. Additionally, one can apply the MG approach to consider two or more inclusions of dielectric constants ϵ_{m1} and ϵ_{m2} with fill factors f_1 and f_2, respectively, in a host medium ϵ_h as[18]

$$\frac{\epsilon_{eff} - \epsilon_h}{\epsilon_{eff} + 2\epsilon_h} = f_1 \frac{\epsilon_{m1} - \epsilon_h}{\epsilon_{m1} + 2\epsilon_h} + f_2 \frac{\epsilon_{m2} - \epsilon_h}{\epsilon_{m2} + 2\epsilon_h} \qquad (2)$$

This equation provides one way to solve multiphase composites.

If we consider the situation that both media of the composites intersperse with each other with equal footing, the BR model is often utilized.[19] In the BR model, two elements are treated equally and their properties are determined self-consistently. The effective dielectric function for a two-phase system is obtained by solving the BR equation,

$$f\left(\frac{\epsilon_m - \epsilon_{eff}}{\epsilon_m + 2\epsilon_{eff}}\right) + (1 - f)\left(\frac{\epsilon_h - \epsilon_{eff}}{\epsilon_h + 2\epsilon_{eff}}\right) = 0 \qquad (3)$$

where notations are the same as those in eq 1. Thus, we have

$$\epsilon_{eff} = \frac{(3f-1)\epsilon_m + (2-3f)\epsilon_h \pm \sqrt{[(3f-1)\epsilon_m + (2-3f)\epsilon_h]^2 + 8\epsilon_h\epsilon_m}}{4}$$
$$(4)$$

where the correct solution is the one with positive effective medium function.

Another very simple mixing model used to describe the distribution of a composite of two elements is so-called simple EMT,[19]

$$\epsilon_{eff}(\omega) = f\epsilon_m(\omega) + (1 - f)\epsilon_h \qquad (5)$$

The detailed discussions about these three models, for instance the validity or applications, have been described well previously.[17−19] For a given material, it is not always clear which EMT model is a better approach for the composites.[18] For extreme cases, with $f = 0$ or $f = 1$, all these models lead to the same result. Of course, if the topology is specified well, it is possible to determine the effective dielectric constant of composite material directly by solving the Maxwell equations numerically. However, experimentally measured dielectric constants combined with some other models are usually of help to determine which method would be used. For ZnO nanostructures studied here, we found that the experimental results of nanowires are described well by the simple EMT, while the BG model shows a good fit to the tubular and prismlike structures,.

Dielectric Models. As described above, our measured samples are the ZnO/air composites, and hence ϵ_h is the dielectric constant of air, giving $\epsilon_h = 1.0$. Next, we need to determine ϵ_m theoretically. Generally, in the terahertz regime, the dielectric function $\epsilon_m(\omega)$ consists of contributions from high-frequency dielectric constant, conduction free electrons, and lattice vibrations,[20,21]

$$\epsilon_m(\omega) = \epsilon_\infty - \frac{\omega_p^2}{\omega^2 + i\gamma\omega} + \sum_j \frac{\epsilon_{st_j}\omega_{TO_j}^2}{\omega_{TO_j}^2 - \omega^2 - i\Gamma_j\omega} \qquad (6)$$

where the first term ϵ_∞ is the high-frequency dielectric constant, the second term describes the contribution of free electrons or plasmons, and the last term stands for the optical phonons. The

key parameters describing the dynamics of free electrons or plasmons in a semiconductor or metal are plasma frequency $\omega_p = \sqrt{Ne^2/(\epsilon_0 m^*)}$ and the carrier damping constant γ, where N is the carrier density, m^* is the electron effective mass, and ϵ_0 is the free-space permittivity constant with a value 8.854×10^{-12} F/m. The mobility can be obtained through the relation $\mu = e/(m^*\gamma)$. In the phonon term, the summation is over all lattice oscillations with the jth transverse optical frequency ω_{TO_j}, oscillator strength ϵ_{st_j}, and phonon damping constant Γ_j. The two most commonly used models can be extracted from eq 6. When the response originates mainly from the contribution of free electrons or plasmons, we usually adopt the Drude model:

$$\epsilon_m(\omega) = \epsilon_{mr} + i\epsilon_{mi} = \epsilon_\infty - \frac{\omega_p^2}{\omega^2 + i\gamma\omega} \qquad (7)$$

The dielectric properties of metals and semiconductors are usually described well by the Drude model.

On the other hand, if the interaction of a radiation field with the fundamental lattice vibration plays a dominant role and results in absorption of electromagnetic wave due to the creation or annihilation of lattice vibration, the dielectric function $\epsilon_m(\omega)$ mainly consists of the contributions from lattice vibrations expressed by the classical pseudo-harmonic phonon model with the first approximation:

$$\epsilon_m(\omega) = \epsilon_{mr} + i\epsilon_{mi} = \epsilon_\infty + \frac{\epsilon_{st}\omega_{TO}^2}{\omega_{TO}^2 - \omega^2 - i\gamma\omega} \qquad (8)$$

where oscillator strength ϵ_{st} is connected to the high-frequency dielectric constant or static dielectric constant ϵ_∞ and the low-frequency dielectric constant or background dielectric constant $\epsilon(0)$ through the relation, $\epsilon_{st} = \epsilon(0) - \epsilon_\infty$. The optical responses of crystals are mostly described well within such a phonon theory framework.

III. Sample Preparation

The detailed fabrication processes about ZnO nanostructures have been described elsewhere.[22] In brief, the tubes were synthesized by decomposing $Zn(NH_3)_4^{2+}$ in ethanol at 180 °C for 13 h, and the prismlike structures were obtained at 100 °C for 13 h with a very similar procedure. The nanowires were prepared using a quaternary microemulsion consisting of 1 g of cetyltrimethylammonium bromide, 1.2 mL of $Zn(OH)_4^{2-}$ solution in 14.3 mL of *n*-hexanol and 10.2 mL of *n*-heptane maintained at 140 °C for 13 h.

X-ray diffraction (XRD) measurements revealed that all the ZnO nanostructures have hexagonal wurtzite structures. The morphologies of these samples were examined by scanning electron microscopy (SEM) and transmission electron microscopy (TEM).[22] The results showed that the diameter of ZnO nanowires is in the range 30−150 nm with a length of up to 3 μm. The inner and outer diameters of the hollow tubes with closed ends are about 250 and 450 nm, respectively. The average length of the tubes is ~4 μm. For the prismlike morphology, the mean diameter and length of the structures are approximately 500 nm and 1 μm, respectively.

IV. THz-TDS Studies

Experimental Methods. The ZnO nanostructures are characterized by use of a photoconductive switch-based THz-TDS system, in which four parabolic mirrors are arranged in an 8-F confocal geometry.[23] A Kerr-lens mode-locked Ti:sapphire laser
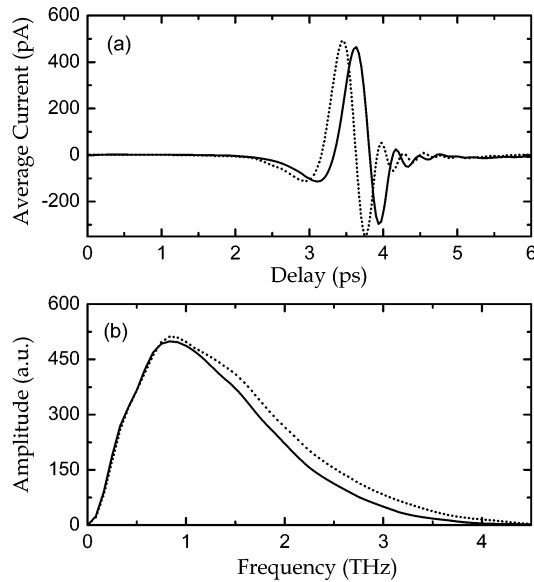
Figure 1. Measured terahertz pulses (a) and the corresponding Fourier transformed spectra (b) of composite ZnO nanowires (solid curve) and reference (dotted curve).

capable of generating 26-fs, 86-MHz femtosecond pulses is used as an excitation source of the THz-TDS. While this confocal configuration enables excellent beam coupling between the transmitter and the receiver, a frequency-independent 3.5-mm-diameter terahertz beam waist is achieved which favors the characterization of samples of small dimensions. The THz-TDS system has a useful bandwidth of 0.1−4.5 THz (3 mm−67 μm) and a signal-to-noise ratio (S/N) of >10000:1. In order to further increase S/N, each curve is an average of six individual measurements.[23]

The transmitted electric field of terahertz pulses through the sample and the reference are recorded in time domain, and the corresponding spectra are obtained by numerical Fourier transform. Figure 1 shows the measured THz-TDS pulses and the corresponding spectra of composite ZnO nanowires and reference. The frequency-dependent absorption, refractive index, and dielectric function of the sample are extracted using the Fourier analysis of the input and output pulses without using the Kramers−Kronig relationship. The complex spectrum of sample pulse $E_2(\omega)$ and the reference spectrum $E_1(\omega)$ are connected through the transfer function,

$$\frac{E_2(\omega)}{E_1(\omega)} = t_{12}t_{21} \exp[id(k - k_0)] \exp(-\alpha_{\text{eff}}d/2) \quad (9)$$

where t_{12} and t_{21} are frequency-dependent complex Fresnel transmission coefficients, d is the sample thickness, α_{eff} is power absorption, $k = 2\pi n_{\text{reff}}/\lambda$ and $k_0 = 2\pi/\lambda$ are the propagation wave vectors, respectively, and n_{reff} is the refractive index of the sample. The frequency-dependent complex dielectric response of the sample is determined by the recorded data of power absorption and refractive index through the relationship, $\epsilon_{\text{eff}}(\omega) = \epsilon_{\text{reff}}(\omega) + i\epsilon_{\text{ieff}}(\omega) = (n_{\text{reff}} + in_{\text{ieff}})^2$, while the imaginary part of the refractive index n_{ieff} is related to power absorption as $n_{\text{ieff}} = \alpha_{\text{eff}}\lambda/4\pi$. As a result, the real and imaginary parts of the dielectric function are given as $\epsilon_{\text{reff}} = n_{\text{reff}}^2 - (\alpha_{\text{eff}}\lambda/4\pi)^2$ and $\epsilon_{\text{ieff}} = \alpha_{\text{eff}}n_{\text{reff}}\lambda/2\pi$, respectively. As described in the EMTs, the measured sample is an effective medium, which is a composite of pure ZnO particles and air. The dielectric function, absorption, and refractive index of the pure ZnO particles can be derived by use of appropriate EMT approaches.
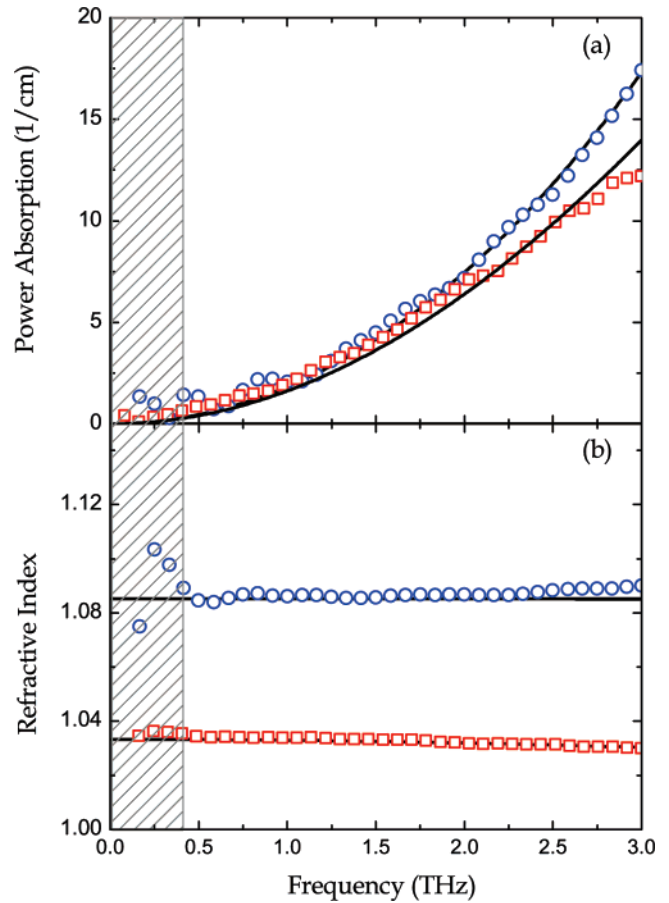

Figure 2. Comparison of THz-TDS measured power absorption and refractive index of ZnO nanowires (circles) and tetrapods (squares) with theoretical fitting (solid curves) calculated using the pseudo-harmonic phonon model by eq 8 combined with the simple EMT model in eq 5. The measurements in shaded areas are not accurate.

THz-TDS of ZnO Nanowires. Figure 2 illustrates the THz-TDS results of ZnO nanowires. The measured absorption coefficients are represented by open circles in Figure 2a. From the relative phase of the spectral components, the refractive index versus frequency is extracted and shown in Figure 2b. The absorption increases steadily with increasing frequencies, and no prominent peaks are observed in the measured frequency range; this is consistent with what is observed in the refractive index, approaching a constant 1.08. The extracted real and imaginary parts of dielectric function of nanowires are depicted by open circles in Figure 3.

As mentioned above, the measured sample is a ZnO−air composite, the complex effective dielectric function can be modeled by the EMT, and the dielectric function of pure ZnO nanostructures can be described by eqs 6−8. The parameters are determined with good accuracy by fitting to the real and imaginary parts of dielectric function, power absorption, and refractive index, simultaneously. By comparing the fitting results with different models, we found that the absorption response of pure ZnO nanowires is mainly attributed to lattice vibration, which is described well theoretically by the classical pseudo-harmonic phonon model in eq 8. Such a phonon model has been utilized in describing the dielectric behaviors of single-crystal ZnO and other materials in the terahertz region.[14,23,24]

Furthermore, we found that the simple EMT of eq 5 used to characterize nanocrystallites[25] and nanoparticles[23] presents a better fit to the measured results of nanowires than other models. As shown by the solid curves in Figures 2 and 3, the measured

Dielectric and Optical Properties of ZnO Nanoforms

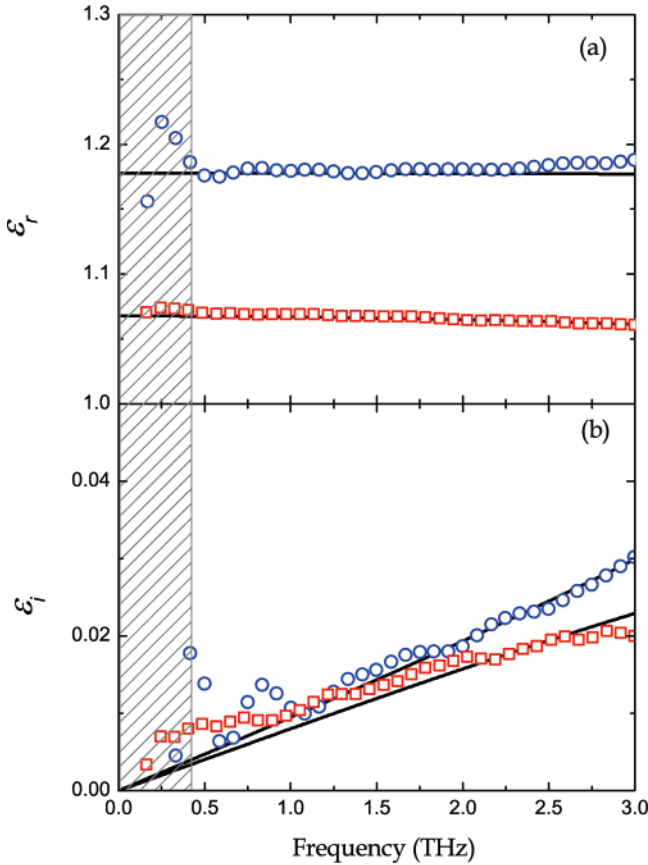*J. Phys. Chem. C, Vol. 111, No. 35, 2007* **13003**

Figure 3. Measured (scatters) and theoretical fitting (solid curves) of real part and imaginary parts of frequency-dependent complex dielectric constants of ZnO nanowires (circles) and tetrapods (squares). The measurements in shaded areas are not accurate.

TABLE 1: Parameters for Theoretical Fitting Calculated Through the Pseudo-harmonic Phonon Model Combined with the Simple EMT Model for ZnO Nanowires and Tetrapods

sample	ϵ_∞	ϵ_{st}	$\omega_{TO}/2\pi$ (THz)	$\gamma/2\pi$ (THz)	f
nanowires	1.75	1.42	12.41 ± 0.2	12.5 ± 0.2	0.082
tetrapods	1.50	3.40	12.41 ± 0.2	21.0 ± 0.2	0.017

power absorption, refractive index, and complex dielectric function of ZnO nanowires are reproduced well by theoretical fit with parameters summarized in Table 1, in which the filling factor is a measured value. The good agreement between the experimental data and theoretical fitting implies that the absorption of nanowires is dominated by the transverse optical mode localized at $\omega_{TO}/2\pi = 12.41 \pm 0.2$ THz, with line width $\gamma/2\pi = 12.5 \pm 0.2$ THz. Such a TO mode at 12.41 THz is a typical transverse optical mode observed previously in the bulk ZnO of wurtzite structure by infrared measurements with assignment of E_1(TO).[26-28] In Figures 2 and 3, the THz-TDS results of ZnO tetrapods (squares) are also presented for comparison.[14] The solid curves represent corresponding theoretical fitting with the same procedure as that for nanowires with parameters shown in Table 1. It is seen obviously that both ZnO nanowires and tetrapods exhibit quite similar behaviors in the terahertz region. Moreover, our recent THz-TDS measurements have also demonstrated that the dielectric properties of single-crystal ZnO is highly related to the transverse optical mode E_1-(TO) at 12.41 THz.[24] Clearly, ZnO nanowires exhibit physical properties similar to those of tetrapod and bulk ZnO crystals.

Further proof also can be found from the Raman spectroscopy measurements shown in section V.

Tubular and Prismlike ZnO. The open circles in Figure 4 show the measured power absorption and refractive index of tubular and prismlike ZnO structures. The absorption features appear to be very similar to those observed in ZnO nanowires and steadily increase with frequencies, but with significantly higher values. At 1.0 THz, the power absorption for both samples is greater than 200 cm^{-1}, and such a highly absorptive feature has essentially limited our measurements to a relatively short frequency range. The refractive index on the other hand, different from what was observed in nanowires, shows a monotonous decrease with increasing frequency. This prominent distinction due to morphologies implicates that the absorption process involves a different response mechanism than that in nanowires. The distinct behaviors also can be observed in the dielectric constants, as illustrated in Figure 5.

As well known, for most metals and doped semiconductors, optical absorption is originated from the interaction of incident light with free carriers, and the common model used to describe such a dielectric response process is the Drude model, as defined in eq 7. The theoretical models used for different ZnO morphologies are determined by the resonance mechanisms denoted in eq 6. If electrons play a dominant role, the Drude model of eq 7 is usually employed. Contrarily, in case the absorption is governed by the interactions between the incident electromagnetic wave and the lattice, the phonon model of eq 8 would be adopted. However, if both response processes have substantial contributions, we would use the overall dielectric model given by eq 6. Considering the contribution of free electrons through the Drude model of eq 7 and the contribution of air from the BG model, we obtain good fits to terahertz spectra of the tubular and prismlike samples with parameters given in Table 2. As shown by the solid curves in Figures 4 and 5, the measured power absorption, index of refraction, and the corresponding complex dielectric constant are well reproduced, indicating that free electrons also play a substantial role in terahertz response of these two structures

A couple of factors can be responsible for such a large difference in behavior between these different ZnO nanostructures. First, the ZnO nanostructures presented here exhibit different morphologies due to different conditions in sample growth. The morphology difference may cause different degrees of crystallization as proved by photoluminescence characterization.[22] Different crystallization in these nanostructures could lead to different densities of structure defects, which in turn result in different carrier concentrations. Second, the existence of tiny ZnO nanoparticles in the content of tubes or around the tubes and prisms can be a source of free electrons.[13,22] Therefore, it is not surprising that the mechanism for the terahertz absorption response of ZnO nanowires is mainly dominated by interaction of incident light with lattice vibrations, while it is ascribed to the contributions from free electrons for tubular and prismlike structures. Furthermore, with electron effective mass $m^* = 0.24$ m_e,[13] the electron density N can be estimated for tubular and prismlike ZnO through the relation $\omega_p = \sqrt{Ne^2/(\epsilon_0 m^*)}$ as 4.2 $\times 10^{18}$ and 1.5×10^{18} cm^{-3}, respectively, little larger than the results measured for the ZnO nanostructures in ref 13. The mobility is obtained as 174 cm^2 V^{-1} s^{-1} for tubes and 119 cm^2 V^{-1} s^{-1} for nanoprisms, which are close to the value of n-type bulk ZnO 205 cm^2 V^{-1} s^{-1} measured by the Hall effect at 300 K.[29] The mobility of materials depends very critically on the type of electron scattering mechanisms, and different scattering
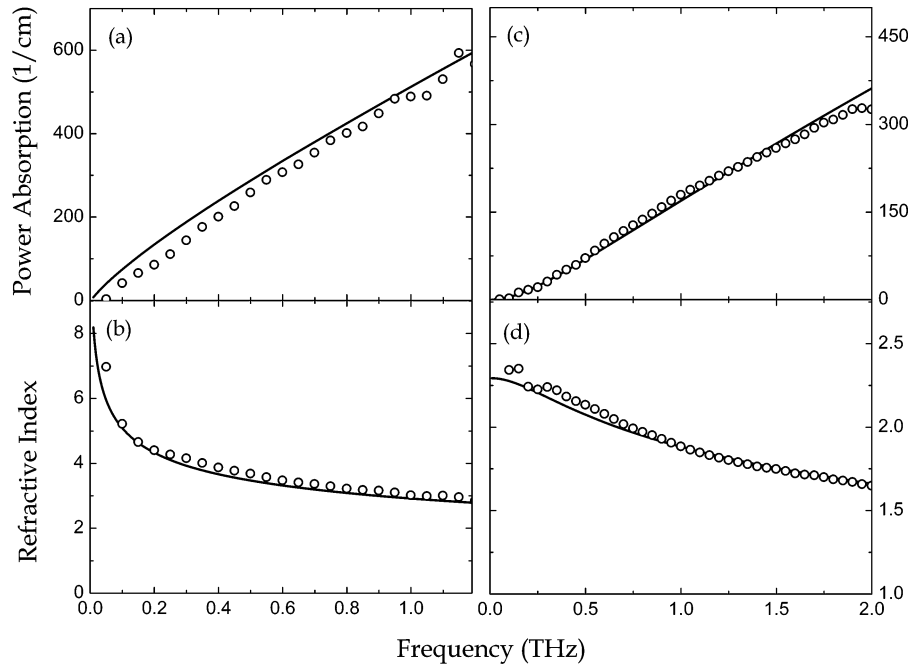
Figure 4. THz-TDS measured (circles) power absorption and refractive index and corresponding theoretical fitting (solid curves) of the tubular and prismlike ZnO structures. Tubes: (a) and (b); prismlike structure: (c) and (d).
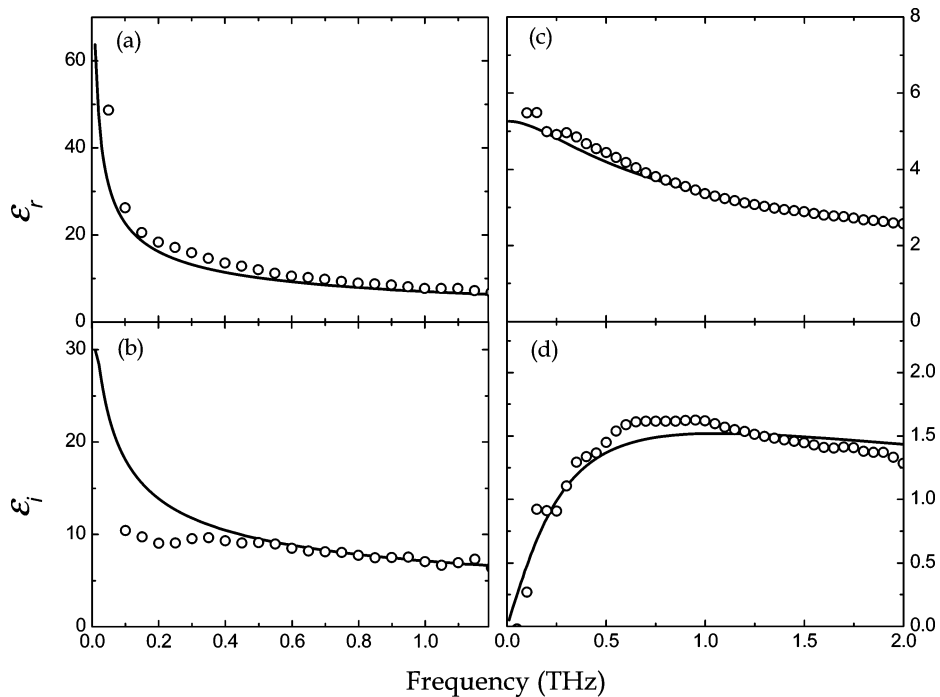

Figure 5. Frequency-dependent complex dielectric function of ZnO nantubes and prismlike structures. Tubes: (a) and (b); prismlike structure: (c) and (d). The solid curves and circles represent theoretical fitting and measurements, respectively.

TABLE 2: Theoretical Parameters for Fitting to Dielectric Function of Tubular and Prismlike ZnO by the Drude Model with Bruggeman Effective Medium Theory

sample	ϵ_∞	$\omega_p/2\pi$ (THz)	$\gamma/2\pi$ (THz)	f
tubes	3.7	37.5 ± 0.2	6.7 ± 0.2	0.33
prisms	3.7	22.5 ± 0.2	9.8 ± 0.2	0.27

laws usually define variable values. Although the morphologies of tubular and prismlike ZnO are different, they have close mobility and this implies that these two structures possess similar physical properties.

V. Raman Spectroscopy Studies

To facilitate in-depth understanding of the far-infrared dielectric and optical properties of these ZnO nanostructures, we also carry out high-resolution Raman spectroscopy characterization. As a supplemental spectroscopy modality here, the Raman spectroscopy confirms the phonon resonances at higher frequencies by extending the frequency range of measurements up to 800 cm^{-1} (24.0 THz). The high-resolution Raman spectra are excited with the 514.5 nm line of an argon ion laser. Figure 6 shows the measured spectra of various ZnO nanostructures in the frequency range from 60 (1.8 THz) to 800 cm^{-1}.
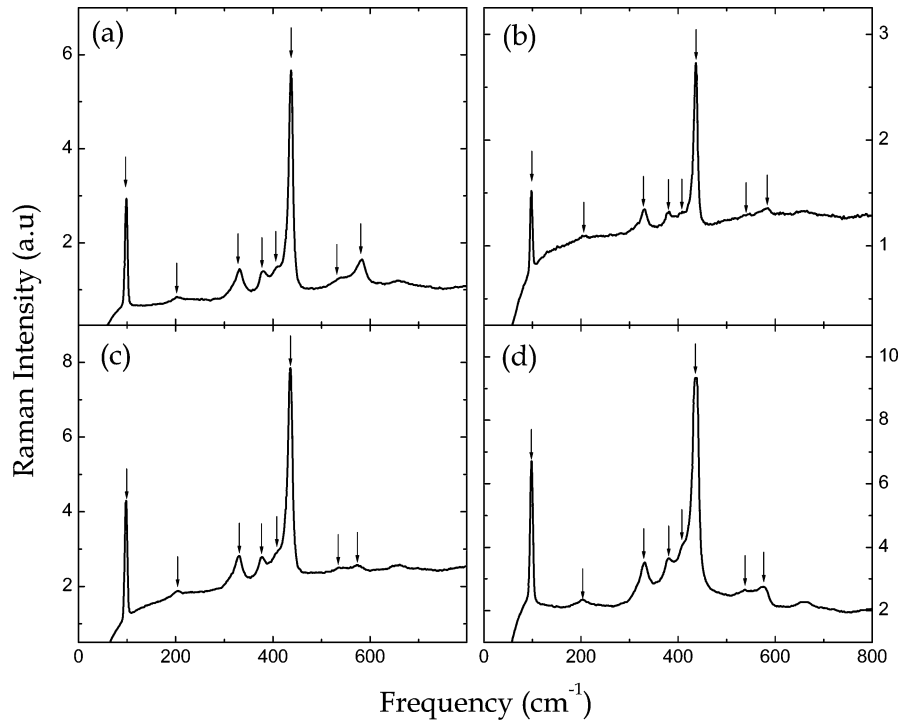
Dielectric and Optical Properties of ZnO Nanoforms

J. Phys. Chem. C, Vol. 111, No. 35, 2007 **13005**

Figure 6. Raman spectra of (a) ZnO nanowires, (b) tetrapods, (c) tubes, and (d) prismlike structures. Each resonance is indicated by an arrow.

The Raman spectra of different ZnO nanomorphologies are quite similar, and all the resonance bands can be well assigned according to the typical optical phonon modes of wurtzite crystal structure.

As one of the II−VI compounds, wurtzite ZnO belongs to the C_{6v}^4 ($P6_3mc$) space group. There are 4 atoms per unit cell leading to 12 phonon branches, 9 optical and 3 acoustic. Group theory predicts the existence of the following optical modes: [26−28] an $A1$ branch, an $E1$ branch, two E_2 branches, and two silent B_1 modes. The A_1 and E_1 are both Raman-active and infrared-active, while E_2 is Raman-active only. Of these phonons, A_1 and E_1 symmetry are polar, and hence A_1 and E_1 branches split into longitudinal optical (LO) and transverse optical (TO) components. As mentioned before, the ZnO nanostructures have been analyzed through SEM, TEM, and XRD. The typical XRD patterns reveal that all these ZnO nanostructures possess hexagonal wurtzite structures. Hence, it is expected that they all present similar phonon responses as confirmed by our Raman scattering measurements. According to the previously reported zone-center optical phonon modes in the wurtzite ZnO, the Raman peaks in ZnO nanostructures are assigned as follows: 98 cm^{-1} to E_2(low), 380 cm^{-1} to A_1(TO), 413 cm^{-1} to E_1(TO), 436 cm^{-1} to E_2(high), 575 cm^{-1} to A_1(LO), and 584 cm^{-1} to E_1(LO). Second-order phonon at 208 cm^{-1}, 334 cm^{-1}, and 539 cm^{-1} are associated with the second-order Raman spectrum due to M point phonons: 2-TA(M), 2-E_2(M), and 2-LA(M), respectively.[3,27−34] Nonpolar phonon modes with symmetry E_2 have two frequencies, E_2(low) and E_2(high), which are related to oxygen atoms and a Zn sublattice.[34] The complete set of measured phonon modes for these nanostructures is summarized in Table 3 in comparison with typical wurtzite single-crystal ZnO.

Compared to bulk materials, nanostructures sometimes present quite dissimilar optical properties mainly arisen from the increase in surface-to-volume ratio, drastic change in electronic structure, and special spatial structures. The evidence for confined optical phonons in ZnO nanoparticles has been revealed by previous Raman scattering investigation.[35] However, from

TABLE 3: Phonon Mode Frequencies (cm^{-1}) of the ZnO Nanowires, Tetrapods, Tubular, and Prismlike Structures, Compared with Those of Bulk Single-Crystal ZnO

sample	single-crystal ZnO	nanowires	tetrapods	tubes	prisms
E_2(low)	102,[a] 101,[b] 98[d]	99	99	98	99
E_2(high)	437,[a] 441,[c] 437.5[d]	437	437	436	437
A_1(TO)	379,[a] 380,[b] 381,[c] 378[d]	379	379	376	379
A_1(LO)	574,[b] 576[d]	583	582	575	576
E_1(TO)	410,[a] 407,[c] 409.5[d]	409	409	408	410
2-TA(M)	208[e,f,g]	205	207	205	205
2-E_2(M)	332[e,f,g]	331	329	331	331
2-LA(M)	541[e,f,g]	539	539	536	538

[a] Ref 25. [b] Ref 26. [c] Ref 27. [d] Ref 28. [e] Ref 29. [f] Ref 30. [g] Ref 23.

the Raman data shown in Figure 6, one can see that these nanostructures preserve almost the overall phonon resonance of bulk single-crystal ZnO with wurtzite structure. This is due to the fact that the dimensions of these structures are much larger than the Bohr radius of ZnO with a calculated value ∼2 nm. The THz-TDS measurements reveal that ZnO nanowires display the behavior similar to that of single-crystal ZnO. However, the tubular and prismlike ZnO show different terahertz absorption features than bulk ZnO due to the fact that their absorption is mainly dominated by electron response. From Figure 6 and Table 3, it is seen that although most of the Raman peaks from the ZnO nanostructures correspond well to those of single-crystal ZnO, the E_1(LO) mode is not observed clearly.

VI. Conclusion

We have studied far-infrared dielectric and optical properties of ZnO nanostructures with different morphologies. Using THz-TDS, we recorded far-infrared power absorption, refractive index, and complex dielectric function of these nanostructures with results well fit by the dielectric models combined with the EMTs. The THz-TDS study implicates that the dielectric function of ZnO nanowires is related to the E_1(TO) phonon mode at 12.41 THz. However, the tubular and prismlike structures exhibit Drude behavior due to the dominant role of

13006 *J. Phys. Chem. C, Vol. 111, No. 35, 2007*

Han et al.

free electrons in the terahertz dielectric response. Furthermore, the low-frequency resonances of Raman scattering by E_1, E_2, A_1, and several second-order modes are characterized. The results indicate that these ZnO nanostructures maintain the overall wurtzite crystal structure and exhibit phonon profiles similar to those of bulk ZnO. The dissimilar and similar properties of different ZnO nanostructures are related to morphologies, crystallization, growth processes, defects, impurities, free carriers, and so on. This study also shows that the combination of THz-TDS with Raman spectroscopy is a favorable approach in understanding low-frequency dielectric properties, optical characteristics, and phonon resonances of nanomaterials.

References and Notes

(1) Wang, Z. L. *J. Phys.: Condens. Matter* **2004**, *16*, 829.

(2) Fan, Z.; Lu, J. G. *J. Nanosci. Nanotechnol.* **2005**, *5*, 1561.

(3) Özgür, Ü.; Alivov, Y. I.; Liu, C.; Teke, A.; Reshchikov, M. A.; Doğan, S.; Avrutin, V.; Cho, S. J.; Morkoç, H. *J. Appl. Phys.* **2005**, *98*, 041301.

(4) Tian, Z. R.; Voigt, J. A.; Liu, J.; Mckenzie, B.; McDermott, M. J.; Rodriguez, M. A.; Kngishi, H.; Xu, H. *Nat. Mater.* **2003**, *2*, 821.

(5) Klingshirn, C. *Chem. Phys. Chem.* **2007**, *8*, 782.

(6) Klingshirn, C.; Hauschild, R.; Fallert, J.; Kalt, H. *Phys. Rev. B* **2007**, *75*, 115203.

(7) Tang, Z. K.; Wong, G. K. L.; Yu, P.; Kawasaki, M.; Ohtomo, A.; Koinuma, H.; Segawa, Y. *Appl. Phys. Lett.* **1998**, *72*, 3270.

(8) Zhang, W.; Wong, K. S.; Wang, H.; Tang, Z. K.; Wong, G. K. L.; Jain, R. K. *Appl. Phys. Lett.* **1999**, *75*, 3321.

(9) Bagnall, D. M.; Chen, Y. F.; Zhu, Z.; Yao, T.; Koyama, S.; Shen, M. Y.; Goto, T. *Appl. Phys. Lett.* **1997**, *70*, 2230.

(10) Ashkenov, N.; Mbenkum, B. N.; Bundesmann, C.; Riede, V.; Lorenz, M.; Spemann, D.; Kaidashev, E. M.; Kasic, A.; Schubert, M.; Grundmann, M.; Wagner, G.; Neumann, H.; Darakchieva, V.; Arwin, H.; Monemar, B. *J. Appl. Phys.* **2003**, *93*, 126.

(11) Ito, Y.; Kushida, K.; Sugawara, K.; Takeuchi, H. *IEEE Trans. Ultrasonics, Ferroelectrics, and Frequency Control* **1995**, *42*, 316.

(12) Ono, S.; Murakami, H.; Quema, A.; Diwa, G.; Sarukura, N.; Nagasaka, R.; Ichikawa, Y.; Oshima, E.; Ogino, H.; Yoshikawa, A.; Fukuda, T. Technical Digest of CLEO' 2005, May 22−27, **2005**, Baltimore, MD (CD ROM), Paper CThX6.

(13) Baxter, J. B.; Schmuttenmaer, C. A. *J. Phys. Chem. B* **2006**, *110*, 25229.

(14) Han, J. G.; Zhu, Z. Y.; Ray, S.; Azad, A. K.; Zhang, W.; He, M.; Li, S.; Zhao, Y. *Appl. Phys. Lett.* **2006**, *89*, 031107.

(15) Fujii, M.; Wada, M.; Kayashi, S.; Yamamoto, K. *Phys. Rev. B* **1992**, *46*, 15930.

(16) Grischkowsky, D.; Keiding, S.; Van Exter, M.; Fattinger, Ch. *J. Opt. Soc. Am. B* **1990**, *7*, 2006.

(17) Granqvist, C. G.; Hunderi, O. *Phys. Rev. B* **1978**, *18*, 2897.

(18) Shalaev, V. M. *Optical Properties of Nanostructured Random Media*; Springer: New York, 2002.

(19) Weissker, H.; Furthmuller, J.; Bechstedt, F. *Phys. Rev. B* **2003**, *67*, 165322; Weissker, H.; Furthmuller, J.; Bechstedt, F. *Phys. Rev. B* **2002**, *65*, 155328.

(20) Balkanski, M. *Optical Properties of Solids*; Abelès, F., Ed.; North-Holland: New York, 1972; Chapter 8.

(21) Han, J. G.; Wan, F.; Zhu, Z. Y.; Liao, Y.; Ji, T.; Ge, M.; Zhang, Z. Y. *Appl. Phys. Lett.* **2005**, *87*, 172107.

(22) Zhang, J.; Sun, L. D.; Pan, H. Y.; Liao, C. S.; Yan, C. H. *New J. Chem.* **2002**, *26*, 33; Zhang, J.; Sun, L. D.; Liao, C. S.; Yan, C. H. *Chem. Commun.* **2002**, *3*, 262; Zhang, J.; Sun, L. D.; Yin, J. L.; Su, H. L.; Liao, C. S.; Yan, C. H. *Chem. Mater.* **2002**, *14*, 4172.

(23) Han, J. G.; Zhang, W.; Chen, W.; Thamizhmani, L.; Azda, A. K.; Zhu, Z. Y. *J. Phys. Chem. B* **2006**, *110*, 1989.

(24) Azad, A. K.; Han, J. G.; Zhang, W. *Appl. Phys. Lett.* **2006**, *88*, 021103.

(25) Weissker, H. Ch.; Fürthmuller, J.; Bechstedt, F. *Phys. Rev. B* **2002**, *65*, 155328.

(26) Decremps, F.; Porres, J. P.; Saitta, A. M.; Chervin, J. C.; Polian, A. *Phys. Rev. B* **2002**, *65*, 092101.

(27) Calleja, J. M.; Cardona, M. *Phys. Rev. B* **1977**, *16*, 3753.

(28) Loudon, R. *Adv. Phys.* **1964**, *13*, 423.

(29) Look, D. C.; Reynolds, D. C.; Sizelove, J. R.; Jones, R. L.; Litton, C. W.; Cantwell, G.; Harsch, W. C. *Solid State Commun.* **1998**, *105*, 399.

(30) Ashkenov, N.; Mbenkum, B. N.; Bundesmann, C.; Riede, V.; Lorenz, M.; Spemann, D.; Kaidashev, E. M.; Kasic, A.; Schubert, M.; Grundmann, M. *J. Appl. Phys.* **2006**, *93*, 126.

(31) Damen, T. C.; Porto, S. P. S.; Tell, B. *Phys. Rev.* **1966**, *142*, 570.

(32) Callender, R. H.; Sussman, S. S.; Selders, M.; Chang, R. K. *Phys. Rev. B* **1973**, *7*, 3788.

(33) Bairamov, B. H.; Heinrich, A.; Irmer, G.; Toporov, V. V.; Ziegler, E. *Phys. Status Solidi B* **1983**, *119*, 227.

(34) Rajalakshmi, M.; Arora, A. K.; Bendre, B. S.; Mahamuni, S. *J. Appl. Phys.* **2000**, *87*, 2445.

(35) Alim, K. A.; Fonoberov, V. A.; Shamsa, M.; Balandin, A. A. *J. Appl. Phys.* **2005**, *97*, 124313.